ELSEVIER

Recovering Surface Temperature and Emissivity from Thermal Infrared Multispectral Data

T. Schmugge, S. J. Hook,† and C. Coll‡*

In 1992 Thermal Infrared Multispectral Scanner (TIMS) data were acquired from the NASA C-130 aircraft over the Sahelian region of West Africa as part of the Hydrological and Atmospheric Pilot Experiment in the Sahel (HAPEX). TIMS measures the radiation from the surface modified by the atmosphere in six channels located between 8 mm and 12.5 μm in the thermal infrared. By using a variety of techniques it is possible to extract both the surface temperature and surface emissivity from the areas over which TIMS data were acquired. One such technique was tested with the data acquired during this experiment. Several TIMS images of both the east and west central sites on 2 and 4 September were processed, and the spectral behaviors of different land cover types were determined. These included tiger bush, millet, and fallow grassland sites. There was a 5–10 K difference in the brightness temperature over the six channels when significant bare soil was visible. Channels 1–3 (8.2–9.4 μm) were cooler than the longer wavelength channels (9.6–12.5 μm), which is characteristic of soils rich in quartz. These differences in brightness were converted to emissivity differences using the max–min difference (MMD) method. This method relies on an empirical relationship observed between the range of emissivities and the minimum value for the six TIMS channels. The MMD method was applied iteratively to several entire scenes for the east central site on the two days with the interesting results that Channel 5 showed very little spatial variation in emissivity and the short wavelength channels observed substantial regions with emissivities of about 0.8 or less. There is excellent reproducibility when the same area is seen in different lines on the same day. However, there are differences when the same area is seen on the two days especially for the low emissivity values. Some of these differences may be due to soil moisture differences of 2–3%, which were observed for the two days. The observed surface temperatures were in good agreement with other measures, for example, vegetation temperatures agreed well with the measured air temperatures. Published by Elsevier Science Inc.

* USDA Hydrology Laboratory, Beltsville
† Jet Propulsion Laboratory, Pasadena
‡ Department of Thermodynamics, Faculty of Physics, University of Valencia, Spain

Address correspondence to T. Schmugge, USDA/ARS Hydrology Lab., Bldg. 007, BARC West, Beltsville, MD 20705. E-mail: schmugge@hydrolab.arsusda.gov

Received 2 September 1997; revised 23 February 1998.

INTRODUCTION

Land surface temperature (LST) and emissivity are key variables for explaining the biophysical processes which govern the balances of water and energy at the land surface. Knowledge of how the fluxes of energy and water vary at the local and regional scale provide boundary conditions for models of atmospheric circulation and water movement in the soils (Bougeault, 1991; Famiglietti et al., 1992). The fluxes are also important controlling influences in models of ecosystem dynamics and crop growth (Choudhury et al., 1986; Gardner et al., 1986; Daughtry et al., 1990; Kustas et al., 1990; Running, 1990; Vidal and Perrier, 1990). An example of the use of remotely sensed LST is given in the recent articles by Humes et al. (1997) and Kustas and Humes (1997). In these articles the authors used LST derived from an airborne radiometer to produce maps of the sensible heat flux over the semiarid Walnut Gulch watershed in the Monsoon 90 experiment. The basic equation for their approach is

$$H=\rho c_p \cdot \frac{T_s - T_a}{r_{ah}}, \tag{1}$$

where ρc_p is the volumetric heat capacity of air, H is the sensible heat flux (W m^{-2}), T_s is the remotely sensed surface temperature, T_a is the air temperature at some reference height, and r_{ah} is the resistance to heat transfer.

REMOTE SENS. ENVIRON. 65:121–131 (1998)
Published by Elsevier Science Inc.
655 Avenue of the Americas, New York, NY 10010

0034-4257/98/$00.00
PII S0034-4257(98)00023-6

In their article Kustas and Humes (1997) were able to scale r_{ah} over the watershed using surface roughness measurements to obtain remotely sensed estimates of H to within 20% of the ground measurements. To obtain this kind of agreement, it is necessary to determine T_s to an accuracy of about 1°C.

Several studies have demonstrated that LST can be recovered from measurements of the emitted radiation in the thermal infrared using airborne and satellite mounted sensors (e.g., Schmugge et al., 1991). However, extraction of the surface temperature from the surface emitted radiation is complicated since the problem is underdetermined and additional assumptions must be made. It is undetermined in that both the temperature and surface emissivity are not known.

Two approaches have been developed to recover LST from multispectral thermal infrared data. The first approach uses a radiative transfer model to correct the at-sensor radiance to surface radiance followed by an emissivity model to break the surface radiance into temperature and emissivity. This approach requires atmospheric profiles from either satellite sounding, conventional radiosondes or model atmospheres for the atmospheric model (Price, 1983, Susskind et al., 1984; Chedin et al., 1985) and an emissivity model which is typically based on laboratory and field measurements (Kealy and Gabell, 1990; Hook et al., 1992; Kealy and Hook, 1993; Matsunaga, 1994). The emissivity model makes certain assumptions about the variation in emissivity with wavelength allowing the under-determined set of equations to be solved. This approach has been adopted for the recovery of LST from the Advanced Spaceborne Thermal Emission Reflectance Radiometer (ASTER) scheduled for launch on the AM-1 platform of the Earth Observing System (Gillespie et al., 1996; Fujisada, 1994).

The second approach involves extending the Sea Surface Temperature (SST) split-window approach to land surfaces (e.g., Price, 1984; Wan and Dozier, 1989; Becker and Li, 1990; Sobrino et al., 1991; Vidal, 1991, Kerr et al., 1992; Ottl and Vidal-Madjar, 1992; Prata, 1994; Coll and Caselles, 1997). This approach assumes the emissivity of the surface in the channels used for the split window is similar, thereby reducing the number of unknowns. This technique works well for some land cover types, that is, those which are gray bodies, such as vegetation, however, large errors can arise over land cover types which have markedly different and unknown emissivities in the split window channels, for example, a quartz-rich soil. This latter approach will be used to produce the temperature and emissivity products for the Moderate Resolution Imaging Spectroradiometer (MODIS), which will also be mounted on the EOS-AM-1 satellite to be launched in late 1998.

This study applies the algorithm currently planned for use with the ASTER instrument to similar data acquired with the Thermal Infrared Multispectral Scanner (TIMS) as part of HAPEX-Sahel (Hydrological and Atmospheric Pilot Experiment in the Sahel). In particular, the effect of atmospheric radiation reflected into the path of the satellite sensor and combined with the emitted radiation on the ASTER algorithm is examined.

MEASUREMENTS

HAPEX-Sahel

HAPEX-Sahel is an international land surface atmosphere observation program that was undertaken in western Niger, in the west African Sahel region (Prince et al., 1995; Goutorbe et al., 1997). The overall aims of the program were to improve our understanding of the role of the Sahel on the general circulation and to seek relationships between the general circulation and the persistent droughts that have affected the Sahel during the last 25 years.

The HAPEX-Sahel field program obtained measurements of atmospheric, surface and certain subsurface processes in a 1°×1° area that incorporates many of the major land surface types found throughout the Sahel. In order to obtain data for this large area, an extensive measurement program was undertaken including field, aircraft, and satellite remote sensing measurements, mainly between mid-1990 and late 1992. An intensive operations period was undertaken for 8 weeks from mid to late growing season of 1992. This included a microwave radiometer for soil moisture observations, a visible and near-IR scanner for vegetation and albedo data and a Thermal Infrared Multispectral Scanner (TIMS) for surface temperature and emissivity. This article deals with the analysis of data from TIMS to obtain values of the surface temperature which can be used in Eq. (1) to obtain estimates of the spatial variation of the surface fluxes.

TIMS: Calibration and Processing

TIMS has six channels in the thermal infrared (8–12 μm) region of the electromagnetic spectrum, an instantaneous field of view is 2.5 mrad and a total field of view of 76.56° (Palluconi and Meeks, 1985). The data presented in this study were acquired on 2 and 4 September 1992 at an altitude of 600 m, yielding a spatial resolution of 1.5m. At this altitude the ground speed exceeded the scan speed, and the data are underscanned, with each scanline being approximately 3 m apart. TIMS undergoes a spectral calibration annually, and the central wavelengths of the channels shift slightly between calibrations. The central wavelengths of the TIMS channels for this experiment were 8.383 μm, 8.785 μm, 9.18 μm, 9.892 μm, 10.733 μm, and 11.655 μm.

For calibration the system is equipped with cold and hot reference sources or blackbodies, whose temperatures are set to span the range of interest. For most of HAPEX experiment the temperature separation between the two

references was set at 30°C. TIMS responds to the incident radiance (W/m^2 sr cm^{-1}) and is related to the brightness temperature of the observed surface via the Planck equation for blackbody radiation.

Initially the TIMS data were calibrated to radiance at the sensor (Palluconi and Meeks, 1985). After calibration the radiance at the sensor (LS) can be written as

$$LS_j=[\varepsilon_j L_j^{BB}(T)+(1-\varepsilon_j)L_j^{sky}]\tau_j+L_j^{atm}, \tag{2}$$

where

ε_j=surface emissivity at wavelength j,
$L_j^{BB}(T)$= spectral radiance from a blackbody at surface temperature T,
L_{jsky}=spectral radiance incident upon the surface from the atmosphere, from MODTRAN,
L_j^{atm}=spectral radiance emitted by the atmosphere, from MODTRAN,
τ_j=spectral atmospheric transmission, from MODTRAN,
LS_j=spectral radiance observed by the sensor.

The radiances at the sensor data were corrected for atmospheric effects to obtain the radiance emitted by the surface [$L_j=\varepsilon_j\, L_j^{BB}(T)$] using the MODTRAN radiative transfer model (Berk et al., 1989). MODTRAN derives values used for the atmospheric correction based on an input atmospheric profile. In this study, local atmospheric data in the form of profiles of relative humidity, temperature, and pressure were acquired from a radiosonde released within a few hours (at most 4) of the overflight (Bessemoulin and Trauille, 1996).

After correction for atmospheric effects including the reflected sky brightness, the radiance from the ground is given by

$$L_j=\frac{(LS_j-L_j^{atm})}{\tau_j}-(1-\varepsilon_j)L_j^{sky}=\varepsilon_j L_j^{BB}(T),$$

$$L_j=\frac{\varepsilon_j C_1}{\lambda_i^5\pi[\exp(C_2/\lambda_j T)-1]}, \tag{3}$$

where

C_1=first radiation constant=3.74151×10^{-16} (W m^2),
C_2=second radiation constant=0.0143879 (m K),
λ_j=wavelength of channel j (m),
T=temperature (K).

If the surface emissivity is known, it is possible to correct for the reflected sky radiation in Eq. (2) and invert Eq. (3) to obtain the surface temperature:

$$T_j=\frac{C_2}{\lambda_i\ln[\varepsilon_j C_1/L_j\lambda_j^5\pi+1]}. \tag{4}$$

Alternatively, the brightness temperature from the ground, assuming an emissivity of 1.0, can be calculated. The ground brightness temperature does not incorporate correction for any reflected sky radiation and therefore can only be compared to similar brightness temperature measurements made at the surface. Such a comparison was done in which the brightness temperatures of part of the Niger River measured with a hand-held radiometer and an immersion thermometer were compared to the surface brightness temperature recovered from two TIMS flight lines. This provides a check on the in-flight calibration of the instrument as well as the accuracy of the atmospheric correction. The brightness temperatures recovered for Channel 5 were within 0.5°C of the measured brightness temperature, indicating that the TIMS was well calibrated and an appropriate amount of atmospheric correction had been applied.

TEMPERATURE/EMISSIVITY RECOVERY

Equation (3) indicates that if the radiance is measured in n spectral channels, there will be $n+1$ unknowns: n emissivities (one per channel) and a single unknown surface temperature. The set of equations described by a set of radiance measurements in n spectral channels is thus underdetermined, and additional information is needed in order to extract either the temperature or emissivity information. This has led to the development of a variety of techniques which differ according to the assumptions that they make. Several techniques have been developed which work better in areas where there is a wide variation in surface emissivity. These include normalized emissivity and alpha emissivity techniques (Gillespie, 1986; Realmuto, 1990; Kealy and Hook, 1993). Recently, a new technique was proposed by Gillespie et al. (1996) which incorporates the advantages of these techniques and is termed temperature emissivity separation (TES). This algorithm is planned for use with data from ASTER. The TES technique is discussed below, detailed descriptions of the other techniques are provided in Kealy and Hook (1993).

Temperature Emissivity Separation (TES)

The following description of the TES algorithm is summarized from Gillespie et al. (1996). The estimated kinetic temperature, T_k, is taken to be the maximum T estimated from the radiances for the n spectral channels:

$$T_k=\max(T_j), \qquad j=1, n, \tag{5}$$

where (T_j) is calculated from Eq. (4). The emissivity value (ε) used in Eq. (4) is set to 0.97 so that typical surface types, vegetation, snow, water, soil, and rock, will all be within ±0.03 of the chosen value. The relative emissivities β_j are then found by ratioing the acquired radiance data, corrected for atmospheric effects to the average of all channels:

$$\beta_j\equiv\frac{L_j\overline{L^{BB}(T)}}{\overline{L}L_j^{BB}(T)}, \tag{6}$$

where

$$\overline{L}=\frac{1}{6}\sum_{j=1}^{6}L_j,$$

$$L_j^{BB}(T)=\frac{C_1}{\lambda_j^5\pi[\exp(C_2/\lambda_j T)-1]},$$

$$\overline{L^{BB}(T)}=\frac{1}{6}\sum_{j=1}^{6}L_j^{BB}(T).$$

In principle, β_j may range widely. However, since the emissivities are generally restricted to 0.7–1.0, the ratioed values are restricted to 0.7–1.4.

The β_j values provide a temperature independent index which can be matched against β_j values calculated from laboratory/field measurements of natural materials. In the TES method the maximum-minimum difference [$\mathrm{MMD}=\max(\beta_j)-\min(\beta_j)$] or contrast is related to the minimum emissivity. A plot of the MMD versus minimum emissivity is given in Figure 1. These values were determined for emissivities measured in the laboratory by Salisbury and D'Aria (1992) with some additional recent measurements for the HAPEX-Sahel soils from the group at the University of Strasbourg (Nerry et al., 1996) and for three soils from the Jornada Desert in New Mexico. The emissivities were also measured by Salisbury. The minimum emissivity is estimated from the observed MMD using

$$\varepsilon_{\min}=0.994-0.687*\mathrm{MMD}^{0.737}, \tag{7}$$

which is derived from a regression fit to the data. This value is used to calculate the emissivities from the β spectrum:

$$\varepsilon_j=\beta_j\left(\frac{\varepsilon_{\min}}{\min(\beta_j)}\right). \tag{8}$$

Figure 1. The MMD–$\varepsilon_{\min}$ relationship, the curve is a plot of Eq. (7).

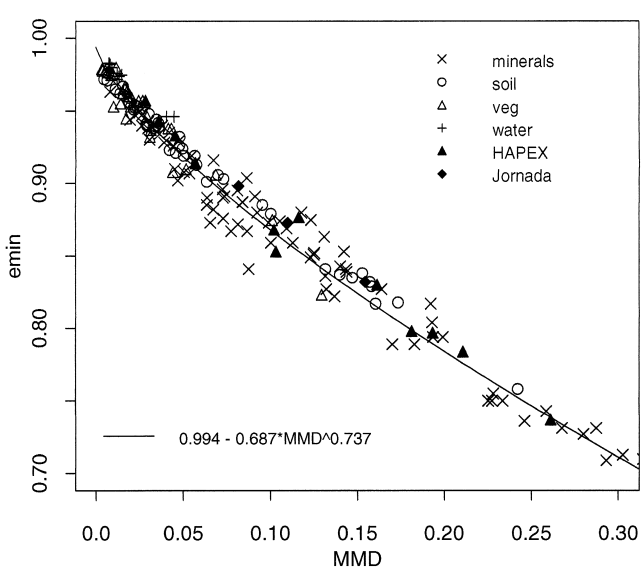

If the emissivities derived with Eq. (8) are used to calculate the temperature from their corresponding original radiance value, the n temperatures will differ slightly if the original temperature estimate was incorrect. An error of 3 K is not uncommon since the maximum emissivity of many materials departs from the assumed emissivity of 0.97. This error can be reduced by calculating the average of the n temperatures and then using the average temperature to recalculate the β_j values. Gillespie et al. (1996) report that using this iterative approach on laboratory data indicate the error can be reduced to a few tenths of a degree. It should be noted that in the current TES approach the iteration is performed after calculation of the normalized temperature prior to calculation of the relative emissivities by ratioing. A final iteration is performed using the emissivities recovered with the MMD. For the cases considered here the results converged after three iterations.

Reflected Atmospheric Radiation

Examination of Eq. (2) indicates that part of the radiance from the ground is reflected atmospheric radiation. In order to correct for this term, that is, to obtain the L_j, the surface emissivity must be known. Since this is rarely the case, either a default value is used or the term is ignored. In the case of dry cold atmospheres, this term is very small since the amount of downwelling atmospheric radiation is small and radiance is reflected as $1-\varepsilon$. Values calculated from MODTRAN radiative transfer model (Berk et al., 1989) are around 1–2% of the at-sensor radiance. However, if the atmosphere is warm and wet, this value can rise substantially. For the 4 September case considered in the next section, the values ranged from 40% to 57% of the at-sensor radiance depending on the channel for the cooler targets. The percentage was largest (>55%) for Channels 1 and 6. The importance of the downwelling radiation was noted in the results from the earlier HAPEX-MOBILHY experiment (Schmugge et al., 1991). In order to correct for this effect, an iterative approach has been proposed by Schmugge and Hook (1995). This involves using the emissivities derived from the chosen temperature/emissivity recovery algorithm to recalculate the ground radiance and rerecover the temperature and emissivity. The recovered temperature and emissivities converge after two or three iterations.

RESULTS

An example of the brightness temperature (T_B) data is given in Figure 2; T_B is the temperature a black body would have for the radiance Ls_j given in Eq. (2). This image is for the east central site (ECS) and shows Channels 5, 3, and 1 displayed in red, green, and blue, respectively. The temperature range is from 30°C to >45°C. The red color in the image is an indication of differences in the emissivity for the exposed bare soil areas. The

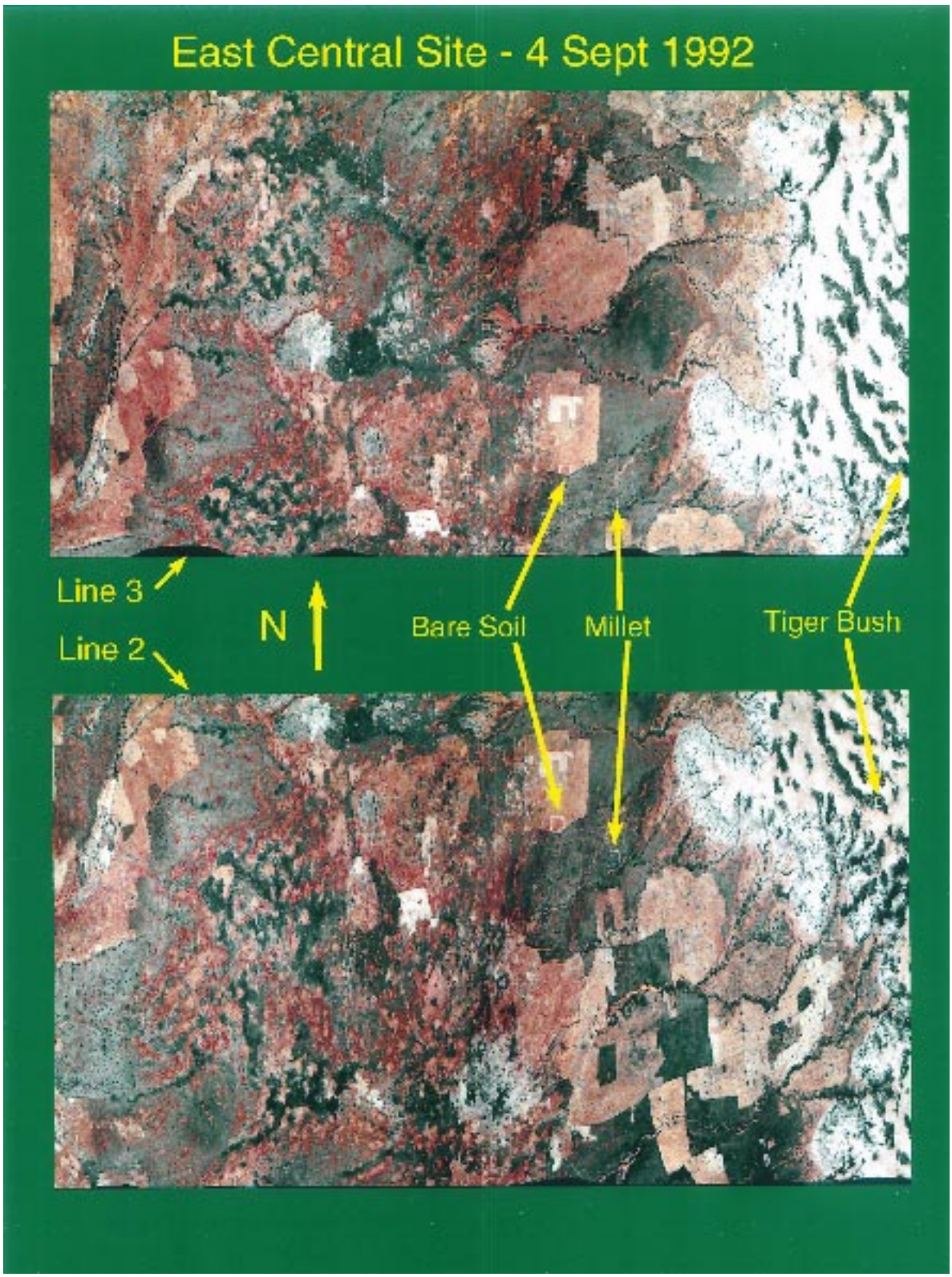

Figure 2. T_B image of the east central site (ECS) for two passes on 4 September 1992. It contains 1000 scans or about 3.2 km in the east-west direction and 900 m across-track. The brightness temperature range is from 30°C to 45°C. Channel 5 is in red, Channel 3 in green, and Channel 1 in blue. The top image is for line 3 and the bottom for line 2. The three targets areas are indicated.

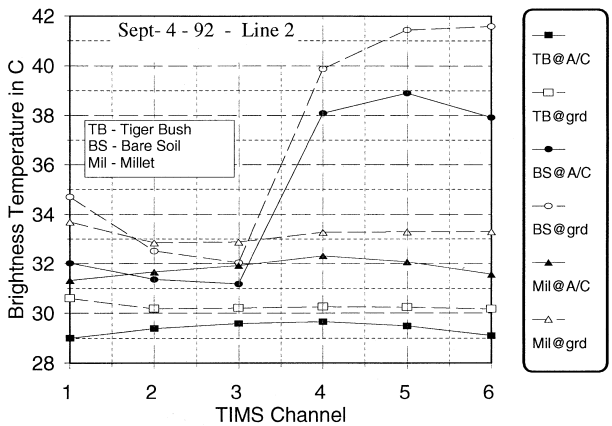

Figure 3. T_B values for three targets at the ECS. The solid symbols are the values at the aircraft and open symbols are the values at the ground, that is, before and after correcting for the effects of the 600 m of atmosphere between the ground and the aircraft.

striped vegetation patterns of the tiger bush is shown on the eastern portion of the scene. There is a transition from the tiger bush plateau to cultivated valleys. This transition or breakaway zone exposes the soil profile typical of a laterite. The radiances for three selected targets (~10–12 pixels each) in the scene for the east central site were obtained from the images. The sites were: a fully vegetated section of the tiger bush, a bare soil and highly vegetated section of a millet field. The brightness temperature values (T_B) before, that is, at the aircraft, and after atmospheric correction are presented in Figure 3. These results are from line 2 on 4 September 1992. They show about a 10 K range of T_B for the bare soil field after correction to a range less than 0.5 K for the tiger bush. The millet shows a little more spectral variation because of the possibility of some bare soil showing. Note that even for a 600 m flight altitude the atmospheric correction was up to 2 K for the bare soil and about 0.5 K for the tiger bush and also that the brightness temperatures at the ground still include the reflected sky brightness. The same area was over flown on line 3 about 20 min later with similar results except that the temperatures were about 1° or 2° warmer. For reference the air temperatures measured at the east Central site on the two days are presented in Table 1 at the times of the overflights. The data are the averages from two stations (Bessemoulin, 1996; Monteny, 1996) separated by a few kilometers. The times of the TIMS overpass are also given. These data indicate that a cool air mass moved through the site on 2 September between the two passes causing the observed temperature difference.

The TES algorithm was applied to the TIMS images with resulting emissivities shown in Figure 4 for Channels 2 and 5 at the same gray scale. Channel 2 has a wide range of emissivities ($0.75 \leq \varepsilon_2 \leq 0.97$) while the range for Channel 5 is much less, indicated by the lack of contrast

Table 1. Air Temperatures at East Central Site in °C

	2 Sept. 1992, Day 246	*4 Sept. 1992, Day 248*
Line 2	30.3@12:50	31.6@13:40
Line 3	25.6@13:20	32.1@14:00

in the image. In the Channel 5 image there is a distinct dark sinuous band near the east edge. The band occurs at a breakaway (Sandy skirt) between the lateritic plateau and surrounding lower ground. At the breakaway the weathering profile of the soil is exposed. This typically consists of a hard surface capping of iron oxides above a mottled zone of iron oxides and kaolinite, and a saprolitic zone of various clays and other secondary minerals. The lower values in the emissivity data for Channel 5 most likely relate to the presence of abundant carbonate and clays exposed in the mottled and saprolitic zones.

The TES derived emissivities for the 3 sites referred to in Figure 3 are presented in Figure 5 for both passes. The solid symbols are the results from line 2 and the open symbols with the dashed lines are for line 3. There is excellent agreement between the two lines. Especially for the bare soil case, where the emissivities for Channels 1, 2, and 3 are about 0.75 in both lines. There is a little more difference for the two vegetation targets especially for the millet field and for the shorter wavelength channels. Note that there are observation differences for the 2 lines; for line 2 the targets were in the northern half of the swath while for line 3 they were in the southern half of the swath. Recall that at the 600 m altitude the scene is underscanned so that only about half of the area is actually seen. Thus, even if the same areas are covered on both lines, slightly different pieces of the terrain may be seen; for example, for the millet field we may be responding to slightly different amounts of bare soil for the millet target on the two flight lines. Also note slight differences in the derived temperatures for all three targets. Line 3 was flown about 20 min later than line 2, and there was a 0.5°C in the air temperature over this interval, not enough to account for the 1–1.5°C difference in the derived temperatures for the vegetation targets. However, for the tiger bush the derived temperatures are within 1°C of the air temperature.

In Figure 6 the bare soil results are compared with emissivity spectra measured for soil samples from the area by the group from the University of Strasbourg (Nerry et al., 1996). The lowest curve is for a soil from one of the millet fields at the ECS. The upper curve is for a sample from the silty crust between the tiger bush rows on the plateau. A sample of TIMS data for a similar location is also shown. These results show that the range of TES derived emissivities is consistent with those expected from the laboratory measurements for the soils from the area.

However, when we compare the data for the same locations on the two days, the agreement is less good as

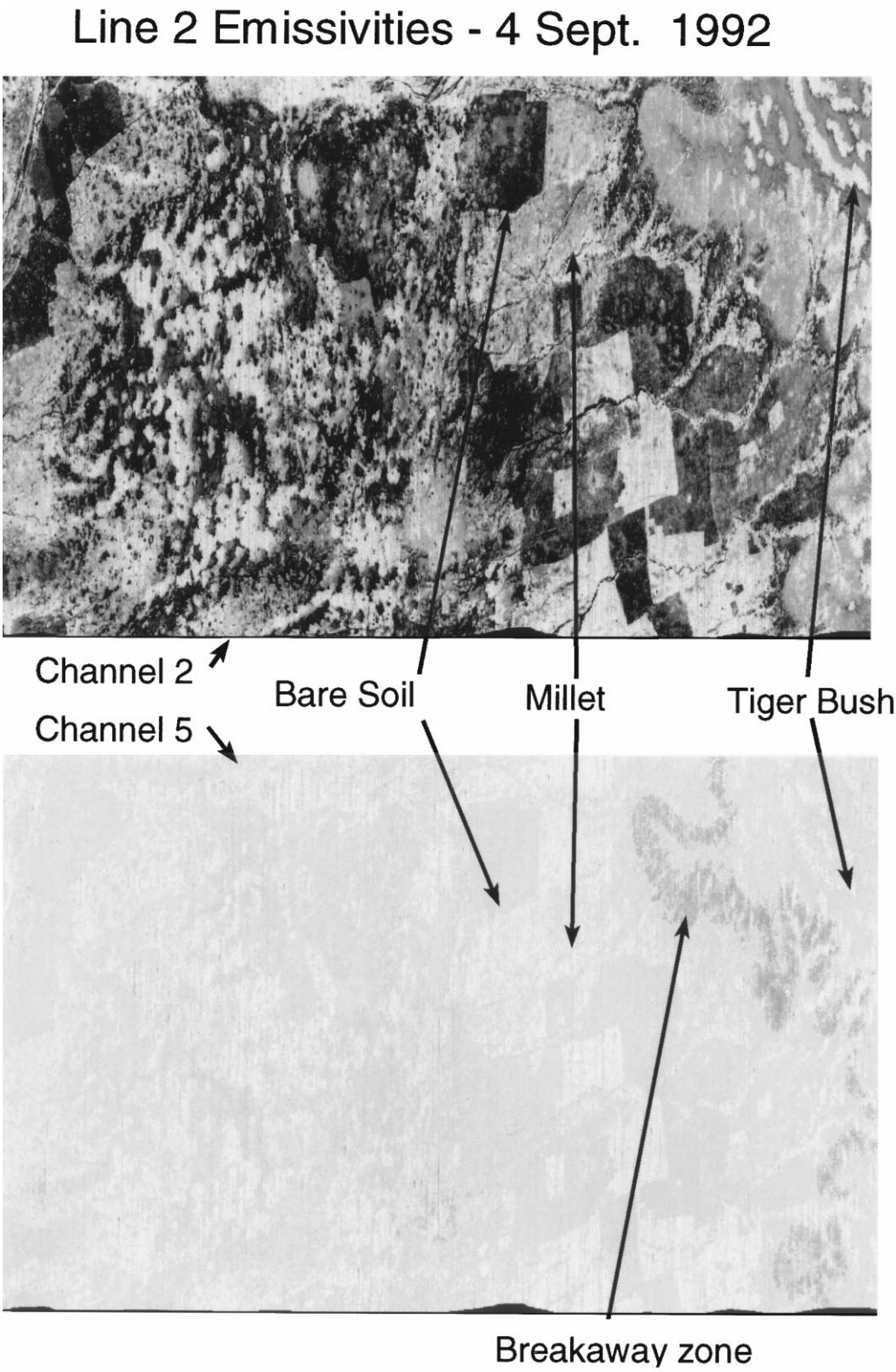

Figure 4. Emissivity images for Channels 2 and 5 derived from the image in Figure 2. The emissivities for both channels are in the same gray scale which ranges from <0.8 (black) to >0.97 (white).

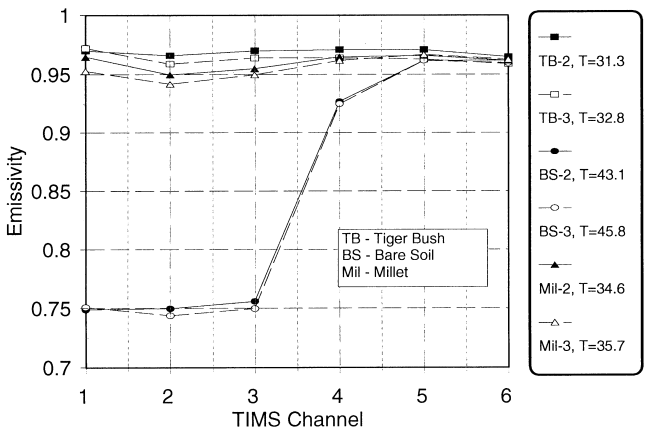

Figure 5. Comparison of derived emissivities for lines 2 and 3 on 4 September 1992 for the ECS. The values of the derived temperature are given in the legend. The solid symbols are line 2 and the open symbols are for line 3.

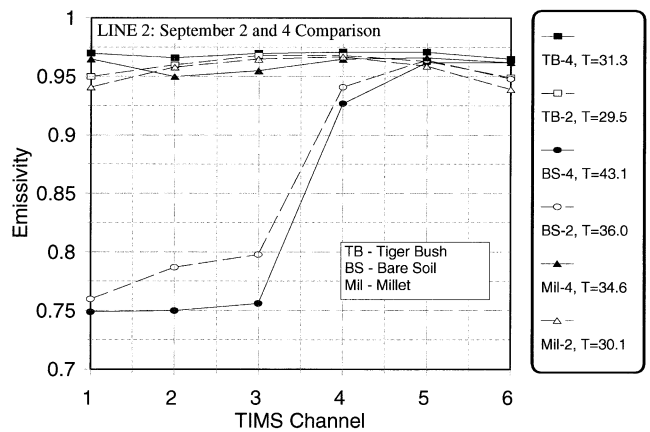

Figure 7. Comparison of derived emissivities for line 2 on 2 and 4 September 1992 for the ECS. The values of the derived temperature are given in the legend. The solid symbols are for 4 September and the open are for 2 September.

seen in Figure 7. Here the open symbols and dashed lines are for the results from 2 September. Again the agreement for the vegetation targets at the longer wavelength channels (4 and 5) is quite good. The agreement is less good for Channels 1 and 6, indicating that the atmospheric correction may not have been as good on 2 September. Also, the derived temperatures were cooler on 2 September. Indeed the sky was cloudier on this day and there was a large temperature difference, ~4°C, observed when lines 2 and 3 were compared for these sites. There was a corresponding decrease in the air temperature between the two passes. In addition to these temperature differences ground measurements of soil moisture at the ECS showed a 2–3% drying between 2 and 4 September (Chanzy et al., 1997). There is also a 14 K increase in the 21-cm microwave brightness temperature between these two days, also indicating a general drying of the soil (Hollenbeck et al., 1996). As Salisbury and D'Aria (1992) have observed, increased soil moisture will increase the emissivity. So perhaps the observed higher emissivity for day 246 is real.

Figure 6. Comparison of laboratory measured emissivity spectra with TES results for bare soil. These measurements were performed by the group from the University of Strasbourg on samples taken from both the east and west central sites.

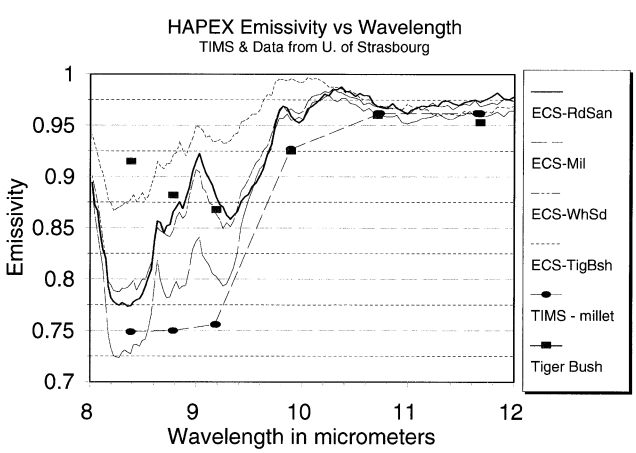

Atmospheric Correction

The sensitivity to atmospheric parameters was tested by varying the relative humidity by ±10% from the measured values for the 4 September case. The idea here is that most of the atmospheric uncertainty will be in water vapor content. We recognize that the low altitude of the flight reduces the effect of the atmosphere; however, there is still a noticeable effect on the MODTRAN output. The MODTRAN results are given in Table 2 and show that varying the atmospheric water content by 10% has about a 10% effect on the atmospheric parameters, e.g., the absorption $(1-\tau)$ increases by about 10% as do the radiation components. The effect of these changes on the derived emissivities are given in Table 3 and shown in Figure 8 for tiger bush in a) and for the bare soil in b). For the tiger bush there is about 0.1 K change in derived temperature and about 0.5 K change for the bare soil. The effect on emissivity is smaller for the tiger bush ~0.005, that is, for the high emissivity targets; for the bare soil target the effect is larger, ~0.03, in Channels 1, 2 and 3. These results give a quantitative indication of the sensitivity of the approach to the atmospheric correction and demonstrate the need for doing this accurately.

DISCUSSION AND CONCLUSION

A version of the TES algorithm was implemented and tested on several 1000-scan TIMS scenes for the east and west central sites in the HAPEX-Sahel experiment. The

Table 2. Atmospheric Parameters Required for Eq. (3) on 4 September 1992 for Three Humidity Levels: as Measured and Multiplied by 1.1 or 0.9[a]

TIMS Channel	As Observed			+10%			−10%		
	τ	L^{atm}	L^{sky}	τ	L^{atm}	L^{sky}	τ	L^{atm}	L^{sky}
1	0.710	2657	5675	0.688	2855	6031	0.732	2453	5300
2	0.818	1731	4381	0.800	1901	4761	0.837	1557	3970
3	0.854	1419	4133	0.836	1587	4542	0.871	1252	3704
4	0.863	1341	4567	0.842	1545	5050	0.883	1147	4092
5	0.825	1673	4815	0.797	1942	5468	0.852	1417	4167
6	0.756	2217	5528	0.720	2537	6190	0.790	1908	4853

[a] The units for L are mW/m^2 sr μm. These values are for a nadir angle 20° which is appropriate for these two targets.

Table 3. Sensitivity of Derived Emissivities to Atmospheric Variations

TIMS Channel	Tiger Bush			Bare Soil		
	ε	$\varepsilon(+10\%)$	$\varepsilon(-10\%)$	ε	$\varepsilon(+10\%)$	$\varepsilon(-10\%)$
1	0.981	0.980	0.982	0.747	0.731	0.759
2	0.976	0.973	0.978	0.748	0.730	0.761
3	0.978	0.975	0.981	0.754	0.736	0.768
4	0.978	0.975	0.981	0.922	0.913	0.926
5	0.978	0.975	0.980	0.958	0.953	0.958
6	0.971	0.970	0.974	0.956	0.958	0.953

scenes were from five different flight lines on 2 and 4 September 1992 from an altitude of 600 m. Results from two of lines are examined in some detail and presented here. There is excellent reproducibility when the same area is seen in different lines on the same day. However, there are differences when the same area is seen on the two days especially for the low emissivity values. Some of these differences may be due to soil moisture differences observed on the two days. The spectral emissivity variations for our soil targets are in qualitative agreement with laboratory measurements made on soils from these sites by the group at the University of Strasbourg and cover about the range of emissivities.

The study illustrates that the TES algorithm is sensitive to any residual atmospheric effects which are not removed. This occurs since any residual atmospheric effects dictate the min–max difference for a spectrally flat target (e.g., vegetation), which in turn will set the minimum emissivity derived from the calibration curve given in Figure 1. In order to minimize residual atmospheric effects, TIMS Channels 1 and 6 were excluded from temperature recovery with the TES calculation. Once

Figure 8. Effects of atmospheric correction uncertainties on the derived emissivities for two sites from line 2 on 4 September 1992. The three curves are for the humidity as measured and for it increased/decreased by 10%. The upper figure is for the tiger bush site and the lower is for Bare Soil site. The derived temperatures are indicated in the legends.

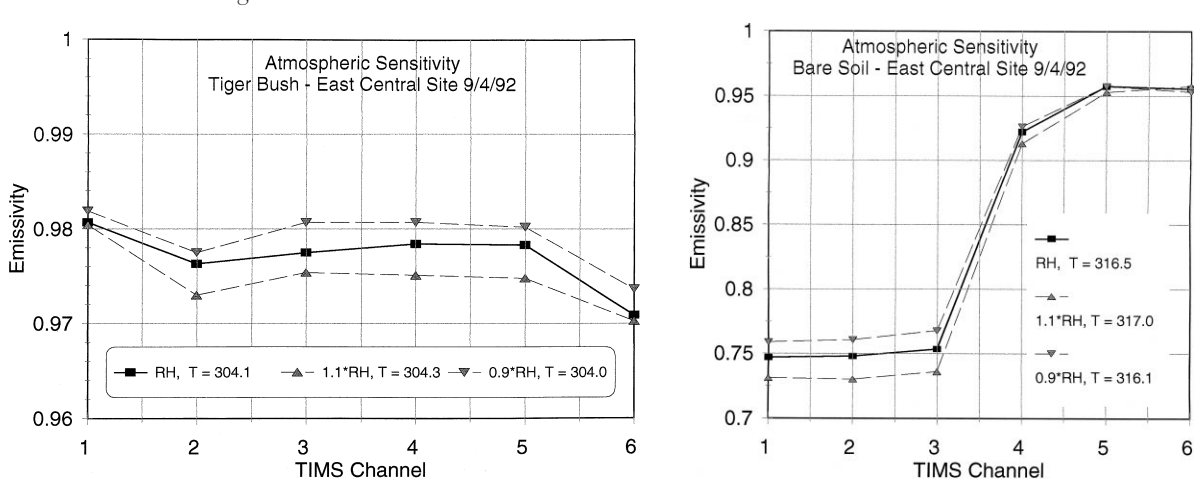

the temperature had been recovered the emissivities were recovered for all channels. These results suggest that using the TES algorithm temperatures and emissivities can be recovered to an accuracy suitable for use in climate modeling and the results are repeatable on different days.

Our results indicated a large sensitivity to the values used for the atmospheric corrections, which in our case was done using MODTRAN 3.5 with nearby radiosoundings of the atmosphere. In particular, we noted the importance of downwelling radiation in determining the emissivity from the observed radiances. An iterative approach has been developed for eliminating the effect of the reflected downwelling radiance. The temperature emissivity extraction technique used is the basis for the approach that will be used with the multispectral thermal data acquired globally by the ASTER instrument and our results illustrate the potential of such data for land studies. The ASTER instrument will fly on-board the EOS-AM1 platform scheduled for launch in late 1998.

We would like to acknowledge the efforts of the several groups whose measurements we used in this activity. These include Bruno Monteny for the ground meteorological measurements, Pierre Bessemoulin of CNRM for the radiosoundings, the group at the University of Strasbourg for the soil emissivity measurements, and the team of the HAPEX-Sahel Information System (HSIS), who have made these data available on CD-Rom.

REFERENCES

Becker, F., and Li, Z.-L. (1990), Toward a local split window method over land surfaces. *Int. J. Remote Sens*. 3:369–393.

Berk, A., Bernstein, L. S., and Robertson, D. C. (1989), MODTRAN: A Moderate Resolution Model for LOWTRAN 7, Tech. Rep. GL-TR-89-0122, Geophys. Lab., HAFB, Bedford, MA.

Bessemoulin, P. (1996), Meteorological data collected by CNRM in the degree square. In *HAPEX SAHEL Ground Data Version 4* (Y. H. Kerr, H. Mahkmara, J. C. Meunier, and T. Valero, Eds.), CD-ROM 3, HSIS LERTS/CNES/ORSTOM, MEDIAS-FRANCE, Toulouse, France.

Bessemoulin, P., and Trauille, O. (1996), Documentation for Radio-sounding data collected by CNRM in Hamdallay, Niger. In *HAPEX SAHEL Ground Data Version 4* (Y. H. Kerr, H. Mahkmara, J. C. Meunier, and T. Valero, Eds.), CD-ROM 3, HSIS LERTS/CNES/ORSTOM, MEDIAS-FRANCE, Toulouse, France.

Bougeault, P. (1991), Parameterization schemes of land-surface processes for mesoscale atmospheric models. In *Land Surface Evaporation* (T. J. Schmugge, and J. C. Andre, Eds.), Springer-Verlang, New York, pp. 93–120.

Chanzy, A., Schmugge, T. J., Calvet, J.-C., et al. (1997), Airborne microwave radiometry on a semi-arid area during HAPEX-Sahel. *J. Hydrol.* 188:287–311.

Chedin, A., Scott, M. A., Wahiche, C., and Moulinier, P. (1985), The improved initialization inversion method: a high resolution physical method for temperature retrievals from the Trios-N series. *J. Clim. Appl. Meteorol*. 24:124–143.

Choudhury, J., Idso, S. B., and Reginato, R. J. (1986), Analysis of a resistive-energy balance method for estimating the evaporation from wheat plots using one-time-of-day infrared temperature observations. *Remote Sens. Environ*. 19:253–268.

Coll, C., and Caselles, V. (1997), A split-window algorithm for land surface temperature from AVHRR data: validation and algorithm comparison. *J. Geophys. Res*. 102(D14):16,697–16,712.

Daughtry, C. S. T., Kustas, W. P., Moran, M. S., et al. (1990), Spectral estimate of net radiation and soil heat flux. *Remote Sens. Environ*. 32:111–124.

Famiglietti, J. S., Wood, E. F., Sivapalan, M., and Thongs, D. J. (1992), A catchment scale water balance model for FIFE. *J. Geophys. Res*. 97:18,997–19,007.

Fujisada, H. (1994), Overview of the ASTER instrument on the EOS-AM1 platform. In *Proc. SPIE*, Vol. 2268, pp. 14–36.

Gardner, B. R., Blad, B. L., and Wilson, G. D. (1986), Characterizing corn hybrid moisture stress sensitivity using canopy temperature measurements. *Remote Sens. Environ*. 19:207–211.

Gillespie, A. R. (1986), Lithologic mapping of silicate rocks using TIMS. In *Proc. TIMS Data User's Workshop*, JPL Publ. 86–38, Jet Propulsion Laboratory, Pasadena, CA, pp. 29–44.

Gillespie, A. R., Rokugawa, S., Hook, S. J. Matsunaga, T., and Kahle, A. B. (1996), Temperature/emissivity separation algorithm theoretical basis document, version 2.1, NASA/GSFC, Greenbelt, MD.

Goutorbe, J. P., Lebel, T., Dolman, A. J., et al. (1997), An overview of HAPEX-Sahel: a study in climate and desertification. *J. Hydrol*. 188–189:4–17.

Hollenbeck, K. J., Schmugge, T. J., Hornberger, G. M., and Wang, J. R. (1996), Identifying soil hydraulic heterogeneity by detection of relative change in passive microwave remote sensing observations. *Water Resour. Res*. 32:139–148.

Hook, S. J., Gabell, A. R., Green, A. A., and Kealy, P. S. (1992), A comparison of techniques for extracting emissivity information from thermal infrared data for geologic studies. *Remote Sens. Environ.*, vol. 42, pp. 123-135.

Humes, K. S., Kustas, W. P., and Goodrich, D. C. (1997), Spatially distributed sensible heat flux over a semiarid watershed. Part I: Use of radiometric surface temperature and a spatially uniform resistance. *J. Appl. Meteor*. 36:281–292.

Kealy, P. S., and Gabell, A. R. (1990), Estimation of emissivity and temperature using alpha coefficients. In *Proc. 2nd TIMS Workshop*, JPL Publ. 90-55, Jet Propulsion Laboratory, Pasadina, CA.

Kealy, P. S., and Hook, S. J. (1993), Separating temperature and emissivity in thermal infrared multispectral scanner data: implications for recovering land surface temperatures. *IEEE Trans. Geosci. Remote Sens*. 31:1155–1164.

Kerr, Y. H., Lagouarde, J. P., and Imberon, J. (1992), Accurate land surface temperature retrieval from AVHRR data with use of an improved split window algorithm. *Remote Sens. Environ*. 41:197–209.

Kustas, W. P., and Humes, K. S. (1997), Spatially distributed sensible heat flux over a semiarid watershed. Part II: Use of a variable resistance approach with radiometric surface temperature. *J. Appl. Meteorol*. 36:293–301.

Kustas, W. P., Moran, M. S., Jackson, R. D., et al. (1990), Instantaneous and daily values of the surface energy balance over agricultural fields using remote sensing and a reference field in an arid environment. *Remote Sens. Environ*. 32: 124–140.

Matsunaga, T. (1994), A temperature–emissivity separation method using an empirical relationship between the mean, the maximum and the minimum of the thermal infrared emissivity spectrum. *J. Remote Sens. Soc. Jpn*. 14(3):28–39.

Monteny, B. (1996), Herbaceous ground flux station data. In *HAPEX SAHEL Ground Data Version 4* (Y. H. Kerr, H. Mahkmara, J. C. Meunier, and T. Valero, Eds.), CD-ROM 3, HSIS LERTS/CNES/ORSTOM, MEDIAS-FRANCE, Toulouse, France.

Nerry, F., Stoll, M. P., and Pion, J. C. (1996), Infrared Spectroradiometry. In *HAPEX SAHEL Ground Data Version 4* (Y. H. Kerr, H. Mahkmara, J. C. Meunier, and T. Valero, Eds.), CD-ROM 3, HSIS LERTS/CNES/ORSTOM, MEDIAS-FRANCE, Toulouse, France.

Ottlé, C., and Vidal-Madjar, D. (1992), Estimation of land surface temperature with NOAA 9 data. *Remote Sens. Environ*. 40:27–41.

Palluconi, F. D., and Meeks, G. R. (1985), JPL Publ. Thermal infrared multispectral scanner (TIMS): an investigator's guide to TIMS data, 85–32, Jet Propulsion Laboratory, Pasadena, CA.

Prata, A. J. (1994), Land surface temperature derived from the advanced very high resolution radiometer and the along-track scanning radiometer 2. Experimental results and validation of AVHRR algorithms. *J. Geophys. Res*. 99(D6): 13,025–13,058.

Price, J. C. (1983), Estimating surface temperature from satellite thermal infrared data—a simple formulation for the atmospheric effect. *Remote Sens. Environ*. 13:353–361.

Price, J. C. (1984), Land surface temperature measurements from the split window channels of the NOAA 7/AVHRR. *J. Geophys. Res*. 89:7231–7237.

Prince, S. D., Kerr, Y. H., Goutorbe, J. P., et al. (1995), Geographical, biological, and remote sensing aspects of the Hydrologic Atmospheric Pilot Experiment in the Sahel (HAPEX-Sahel). *Remote Sens. Environ*. 51:215–234.

Realmuto, V. J. (1990), Separating the effects of temperature and emissivity: emissivity spectrum normalization. In *Proc. 2nd TIMS Workshop*, JPL Publ. 90–55, Jet Propulsion Laboratory, Pasadena, CA.

Running, S. W. (1990), Estimating terrestrial primary productivity by combining remote sensing and ecosystem simulation. In *Remote Sensing of Biosphere Functioning* (R. Hobbs and H. Mooney, Eds.), Springer-Verlag, New York, pp. 65–68.

Salisbury, J. W., and D'Aria, D. M. (1992), Emissivity of terrestrial materials in the 8–14 μm atmospheric window. *Remote Sens. Environ*. 42:83–106.

Schmugge, T., and Hook, S. J. (1995), Recovering surface temperature and emissivity from thermal infrared data. In *American Geophysical Union 1995 Fall Meeting*, San Francisco, p. F132.

Schmugge, T. J., Becker, F., and Li, Z.-L (1991), Spectral emissivity variations observed in airborne surface temperature measurements. *Remote Sens. Environ*. 35:95–104.

Sobrino, J. A., Coll, C., and Caselles, V. (1991), Atmospheric correction for land surface temperature using NOAA 11 AVHRR. *Remote Sens. Environ*. 38:19–34.

Susskind, J., Rosenfield, J., Reuter, D., and Chahine, M. T. (1984), Remote sensing of weather and climate parameters from HIRS2/MSU on TIROS-N. *J. Geophys Res*. 89(D3): 4677–4697.

Vidal, A. (1991), Atmospheric and emissivity corrections of land surface temperature measured from satellite using ground measurements or satellite data. *Int. J. Remote Sens*. 12: 2449–2460.

Vidal, A., and Perrier, A. (1990), Irrigation monitoring by following the water balance from NOAA-AVHRR thermal infrared data. *IEEE Trans. Geosci. Remote Sens*. 28(5):413–421.

Wan, Z.-M., and Dozier, J. (1989), Land surface temperature measurement from space: physical principles and inverse modeling. *IEEE Trans. Geosci. Remote Sens*. 27:268–278.